Published in final edited form as:
Biochim Biophys Acta. 2014 February ; 1842(2): 220–231. doi:10.1016/j.bbadis.2013.11.009.

Inhibition of ERK-DLP1 signaling and mitochondrial division alleviates mitochondrial dysfunction in Alzheimer's disease cybrid cell

Xueqi Gan[1,2], **Shengbin Huang**[1,2], **Long Wu**[1], **Yongfu Wang**[1], **Gang Hu**[1], **Guangyue Li**[1,2], **Hongju Zhang**[1], **Haiyang Yu**[2], **Russell Howard Swerdlow**[3], **John Xi Chen**[4], and **Shirley ShiDu Yan**[1,*]

[1]Department of Pharmacology and Toxicology, and Higuchi Bioscience Center, School of Pharmacy, University of Kansas, Lawrence, KS 66047

[2]State Key Laboratory of Oral Diseases, West China Hospital of Stomatology, Sichuan University, Cheng Du, China 610041

[3]Department of Neurology, University of Kansas Medical Center, Kansas City, KS 66160

[4]Department of Neurology, Memorial Sloan-Kettering Cancer Center, New York, NY 1003

Abstract

Mitochondrial dysfunction is an early pathological feature of Alzheimer's disease (AD). The underlying mechanisms and strategies to repair it remain unclear. Here, we demonstrate for the first time the direct consequences and potential mechanisms of mitochondrial functional defects associated with abnormal mitochondrial dynamics in AD. Using cytoplasmic hybrid (cybrid) neurons with incorporated platelet mitochondria from AD and age-matched non-AD human subjects into mitochondrial DNA (mtDNA)-depleted neuronal cells, we observed that AD cybrid cells had significant changes in morphology and function; such changes associate with altered expression and distribution of dynamin-like protein (DLP1) and mitofusin 2 (Mfn2). Treatment with antioxidant protects against AD mitochondria-induced extracellular signal-regulated kinase (ERK) activation and mitochondrial fission-fusion imbalances. Notably, inhibition of ERK activation not only attenuates aberrant mitochondrial morphology and function but also restores the mitochondrial fission and fusion balance. These effects suggest a role of oxidative stress-mediated ERK signal transduction in modulation of mitochondrial fission and fusion events. Further, blockade of the mitochondrial fission protein DLP1 by a genetic manipulation with a dominant negative DLP1 (DLP1^{K38A}), its expression with siRNA-DLP1, or inhibition of mitochondrial division with mdivi-1 attenuates mitochondrial functional defects observed in AD cybrid cells. Our results provide new insights into mitochondrial dysfunction resulting from

*Corresponding author: Shirley ShiDu Yan M.D, Departments of Pharmacology and Toxicology and Higuchi Bioscience Center, School of Pharmacy, University of Kansas, 2099 Constant Ave., Lawrence, KS 66047, USA, shidu@ku.edu, Tel: 1-785-864-3637.

Conflict of Interest: The authors have no conflict of interest to disclose

changes in the ERK-fission/fusion (DLP1) machinery and signaling pathway. The protective effect of mdivi-1 and inhibition of ERK signaling on maintenance of normal mitochondrial structure and function holds promise as a potential novel therapeutic strategy for AD.

Keywords

Mitochondrial fission and fusion; Alzheimer's disease; Cybrid cells; ERK; DLP1

1. Introduction

Alzheimer’s disease (AD) is the most common form of dementia characterized clinically progressive cognitive decline and neuronal loss. Pathologically, AD-affected brain shows accumulation of amyloid beta peptide (Aβ) and neurofibrillary tangles with tau hyperphosphorylation. Recent studies indicate that mitochondrial dysfunction, an early pathological feature in AD, plays a central role in its pathogenesis of AD [1–6]. Perturbed bioenergetic function, especially mitochondrial dysfunction, is seen in brain and peripheral tissues of subjects with AD [7, 8]. Cytochrome c oxidase (CcO) activity is lower in human AD platelet mitochondria [8–10]. Neurons are especially vulnerable to mitochondrial dysfunction due to inherent high energy demands and dependence on respiration for ATP generation [3, 11]. Thus, mitochondrial dysfunction may drive or mediate various AD pathologies.

Mitochondria are dynamic organelles that undergo continuous fission and fusion. These processes are regulated by the large dynamin-related GTPases mitofusin 1 and 2 (Mfn1 and 2), and optic atrophy1 (OPA1) for fusion and dynamin-like protein (DLP1) for fission [12, 13]. Mitochondrial dynamics play an essential role in ensuring appropriate distribution of mitochondria within cells, a function that is particularly critical for morphologically complex cells such as neurons [14]. Alterations in mitochondrial dynamics significantly impact almost all aspects of mitochondrial function including energy metabolism, calcium buffering, reactive oxygen species (ROS) generation and apoptosis regulation [12, 15]. Imbalance of mitochondrial fission and fusion is an important mechanism in neurodegenerative diseases including Parkinson disease (PD), Huntington disease (HD), and AD. Although it has been demonstrated that altered mitochondrial fission or fusion is involved in Aβ-mediated mitochondrial morphological changes leading to neuronal and synaptic dysfunction in a transgenic AD mouse model and *in vitro* cell culture [15–17], the direct consequences and mechanisms underlying AD-derived mitochondrial defects on mitochondrial dynamics and associated mitochondrial function have not been fully elucidated. The following questions arise: Do AD-derived mitochondria show changes in mitochondrial fission and fusion events? If so, are these altered mitochondrial dynamics associated with mitochondrial dysfunction? Does inhibition of abnormal mitochondrial fusion and fission rescue aberrant mitochondrial morphology and function? Thus, it is essential to uncover the mechanism by which AD mitochondria modulate this vital mitochondrial process.

To explore the mechanisms associated with AD-specific mitochondrial defects, we used cybrid cells with incorporated platelet mitochondria from AD or age-matched non-AD human subjects into mitochondrial DNA (mtDNA)-depleted neuronal cells (SH-SY5Y). The resulting cell lines, referred to as AD or non-AD cybrids, have been demonstrated to have different bioenergetic profiles [7]. AD cybrids recapitulate many potential pathogenic features of AD, such as decreased activity associated with respiratory chain key enzyme, increased free radical production rates, and other functional changes that likely arise as a consequence of perturbed respiratory chain function typically observed in AD brain mitochondria [18, 19].

Using AD cybrids, we comprehensively evaluated the consequences of changes in AD-specific mitochondria on mitochondrial dynamics and mitochondrial function. We further delineated the mechanism by which AD mitochondria regulate mitochondrial fission/fusion events. Our investigation provides new insight into the role of mitochondrial dynamics in AD pathogenesis, highlighting the potential diagnostic and therapeutic application for AD.

2. Material and methods

2.1 Human subjects and creation of cybrid cell lines

Individuals for this study were recruited from the University of Kansas Alzheimer's Disease Center. AD subjects met the National Institute of Neurological and Communicative Disorders and Stroke and the Alzheimer's Disease and Related Disorders Association criteria [20]. Non-AD subjects were cognitively normal and age-matched to AD subjects. This study was approved by the University of Kansas Medical Center (KUMC) Institutional Review Board. All subjects provided written informed consent to participate in the study. The ages of AD and non-AD subject platelet donors were 73.3 ± 2.6 and 74 ± 2.9 years, respectively. Gender, age and disease status of donor patients are presented in supplemental Table. S1.

Cybrid cell lines were created on the human neuroblastoma cell (SH-SY5Y) nuclear background (by the KU ADC Mitochondrial Genomics and Metabolism Core) [21]. To create the cybrid cell lines used for this study, SH-SY5Ycells that were previously depleted of endogenous mtDNA (Rho0 cells) were fused with the platelet cytoplasm and repopulated with mitochondria containing mtDNA from patients or controls as previously described [22]. Briefly, Rho0 cells were incubated with donor platelets in a DMEM-polyethylene glycol solution. Immediately after this, cells were initially placed in Dulbecco's Modified Eagle Medium (DMEM) supplemented with 10% non-dialyzed fetal bovine serum (FBS), 200μg/ml sodium pyruvate, 150 μg/ml uridine, and 1% penicillin–streptomycin solution to recover. Seven days after the fusion event, cells were switched to a selection medium containing 10% dialyzed fetal calf serum but lacking pyruvate and uridine. These conditions resulted in selection against Rho0 cells that were not repopulated with donor mitochondria. Only cells containing patient's platelet mtDNA can regain aerobic competence and survive the subsequent selection processes. Following selection, each cybrid cell line was maintained in medium containing DMEM supplemented with 10% non-dialyzed FBS and 1% penicillin-streptomycin solution in a humidified 95% air/5% CO2 incubator at 37°C for over 2 months. The quantitative real-time PCR showed that the intact mtDNA copies were

present in all cybrids without detectable large scale deletion after many passages of cell proliferation (Fig. S1).

Cells were treated with probucol (10 μM) (Sigma), ERK1/2 inhibitor PD98058 (10 μM) (Sigma), or mitochondrial division inhibitor mdivi-1 (10 μM) (Sigma) for 24 h prior to biochemical and molecular assays.

2.2 Measurement of enzyme activities associated with respiratory chain complexes

Briefly, cybrid cells were washed with ice-cold PBS, and then harvested, centrifuged, and suspended in 50 μL of isolation buffer containing 250 mM sucrose, 20 mM HEPES, and 1 mM EDTA. Cell suspensions (containing ~3–4 mg of protein/ml) were added to a cuvette containing 0.95 mL of 1× assay buffer (10 mM Tris-HCl, and 120 mM KCl), and the reaction volume was brought to 1.05 mL with the addition of 1× enzyme dilution buffer (10 mM Tris-HCl, pH 7.0). The reaction was then initiated by addition of 50 μL of ferrocytochrome substrate solution (0.22 mM), and the change in absorbance of cytochrome c at 550 nm was measured using a Shimadzu (Kyoto, Japan) UV1200 spectrophotometer. Activity is expressed as micromoles of cytochrome oxidized per min^{-1} mg^{-1} protein using an extinction coefficient of 27.84 mM^{-1} cm^{-1}. Enzyme activities in complex I (NADH-ubiquinone reductase), complex II (succinate dehydrogenase), complex III (ubiquinol-cytochrome c reductase), complex IV (cytochrome c oxidase, CcO) and citrate synthase activity were determined as described previously [23, 24].

2.3 Measurement of ATP levels

ATP levels were determined using an ATP Bioluminescence Assay Kit (Roche) following the manufacturer's instructions [2, 25]. Briefly, cells were harvested using the provided lysis buffer, incubated on ice for 15 min, and centrifuged at 13,000 g for 10 min. ATP levels were measured using a Luminescence plate reader (Molecular Devices) with an integration time of 10 s.

2.4 Functional imaging

Cybrid cells were harvested from 75 cm^2 flasks and replated at low density onto Lab-Tek eight-well chamber slides. Mitochondrial ROS generation was determined using Mitosox Red (Molecular Probes), a unique fluorogenic dye highly selective for detection of superoxide production in live cell mitochondria. Cells were incubated with fresh growth medium containing 2.5 μM Mitosox for 30 min. For mitochondrial membrane potential determination, cells were co-stained with Mitotracker Green (MTGreen) (100 nM; Molecular Probes) and TMRM (100 nM; Molecular Probes) for 30 min. Fluorescence from MTGreen is independent of membrane potential, whereas TMRM is sensitive to membrane potential. Mitochondria were labeled with Mitotracker Red (Molecular Probes, incubated in 100 nM Mitotracker Red for 30 min at 37 °C before fixation) to visualize morphology.

Images were captured under a microscope (Leica TCS SPE) using a 63X 1.4 NA Apochrome objective (Carl Zeiss MicroImaging, Inc.). Excitation wavelengths were 543 nm for Mitosox, TMRM or Mitotracker Red, and 488 nm for MTGreen, respectively. Fluorescent signals were quantified using NIH Image J software. Post-acquisition processing

was performed with MetaMorph (Molecular Devices) and NIH Image J software for quantification and measurement of fluorescent signals of mitochondrial length and occupied area. Mitochondrial size, shape, density, and fluorescent intensity were quantified by an investigator blinded to experimental groups. More than 100 clearly identifiable mitochondria from randomly selected 10–15 cells per experiment were measured in 3 independent experiments.

2.5 Isolation of mitochondria and immunoblot analysis

Mitochondrial fraction and cytosol isolated from cybrid cells were suspended in buffer (150 mM KCl, 5 mM HEPES, 2 mM K_2HPO_4, 5 mM glutamate, 5 mM malate, 150 mM potassium thiocyanate, pH 7.2), and subjected to the immunoblotting. The rabbit anti-DLP1 (1:3000, Thermo scientific), mouse anti-Mfn2 (1:2000, Sigma), mouse anti-Hsp60 (1:5000, Enzo), rabbit anti-phospho-ERK1/2, mouse anti-ERK1/2 (1:2000, Cell signaling), and mouse anti-β-actin (1:8000, Sigma) were used as primary antibodies. Binding sites of primary antibody were visualized with horseradish peroxidase-conjugated anti-rabbit IgG antibody (1:5000, life technology) or anti-mouse IgG antibody (1:5000, life technology) followed by the addition of enhanced chemiluminescence (ECL) substrate (GE Healthcare). We quantified relative optical density of immunoreactive bands using NIH Image J software.

2.6 Mdivi-1 Treatment

Mdivi-1 was dissolved in DMSO (50 mM) and diluted with culture medium to the working concentration. Cells were treated with mdiv-1 (10 μM) for 24–48 h, and mitochondrial density, length, morphology, CcO activity, and ATP levels were determined as described above.

2.7 Transient Transfection of mitochondrial fission construct (DLP1^{K38A})

Cells were transfected with plasmids containing GFP-tagged DLP1^{K38A} (provided by Dr. Yi-Ren Hong, Kaohsiung Medical University Hospital, Taiwan) or GFP-tagged empty vector alone using Lipofectamine 2000 (Invitrogen) according to manufacturer's instructions. Forty-eight hours after transfection, cells were assessed for changes in mitochondrial morphology or ATP levels as described above. Transfected cells were visualized with green fluorescent protein (GFP) as reported [26].

2.8 Knockdown of DLP1 expression by siRNA-DLP1

The cybrid cells were transfected with SiRNA targeting human DLP1 (accession number NM012062) or control siRNA (ON-TARGET Plus SMART Pool™, Dharmacon Research) using Oligofectamine (Invitrogen) according to the manufacturer's instructions. DLP1 silencing efficiency was evaluated by immunoblotting of DLP1 protein expression at 48 h after siRNA transfection. In the parallel experiments, the mitochondrial morphology was detected by immunostaining and Mitotracker Red staining.

2.9 Statistical analysis

Data are presented as mean ± SEM. Statistical analysis was performed using Statview software (SAS Institute, Version 5.0.1). Differences between means were assessed by Student's *t*-test or one-way analysis of variance (ANOVA) with Bonferroni/Dunn posthoc test. $P < 0.05$ was considered significant.

3. Results

3.1 Mitochondrial Dysfunction in AD Cybrid Cells

We first characterized mitochondrial function by evaluating key enzymes associated with respiratory chain, membrane potential, and bioenergy in newly created cybrid neuronal cells containing AD or age-matched non-AD platelet mitochondria. Compared to non-AD cybrids, AD neurons had a significant decrease in complex I, III, and IV activities (Fig. 1*A–C*). No significant change in complex II activity was found in AD cybrid cells (Fig. S2*A*). Similarly, ATP levels were reduced by 40–50% in AD cybrid cells (Fig. 1*D*). Citrate synthase activity, used as a quantitative enzyme marker for the presence of intact mitochondria, was comparable between AD and non-AD cybrids (Fig. *S2B*).

To more carefully evaluate mitochondrial function, we measured inner mitochondrial membrane potential ($\Delta m\Psi m$). Cells were treated with tetramethylrhodaminemethylester (TMRM) to monitor mitochondrial membrane potential. TMRM staining was significantly decreased in AD cybrids by 50–60% compared to non-AD cybrids (Fig.1*E*).

Given that mitochondria are a major source of ROS generation and that ROS accumulation affects mitochondrial function, we tested whether mitochondrial ROS generation correlates with mitochondrial dysfunction. Indeed, the intensity of Mitosox staining, an indicator for mitochondrial ROS, was significantly increased in AD cybrids compared to non-AD control cybrids (Fig. 1*F*).

3.2 Abnormal Mitochondrial Morphology and Mitochondrial Fission/Fusion Events in AD Cybrid Neurons

Next, we evaluated changes in mitochondrial distribution and morphology. Mitochondrial density in whole cell, cell body, and process was decreased in AD cybrid cells compared to non-AD cells (Fig. 2*A1–A3*). Decreased mitochondrial density was more severe in processes than in cell bodies (decreased by 40–50% in processes *vs.* 25–30% in cell bodies of AD cybrids compared to non-AD (Fig. 2*A2–A3*). Morphologically, mitochondria in non-AD cybrids were rod-like or elongated, and regularly distributed (Fig. 2*B*), whereas mitochondria were fragmented, misshapen, bleb-like, and collapsed away from the mitochondrial network in AD cybrid cells (Fig. 2*B*). Accordingly, mitochondrial length was significantly shorter in AD cybrids than in non-AD controls (Fig. 2*C1–C4*), particularly in neuronal process regions (Fig. 2*C2*).

Balance of mitochondrial fission and fusion proteins is critical for maintenance of normal mitochondrial morphology [17, 27]. DLP1 is a key player in mitochondrial fission regulation acting directly or indirectly with other fission/fusion proteins, and its

translocation to mitochondria initiates the fission process [28]. Mitochondrial fraction and cytosol from each cybrid cell line were isolated to assess fission and fusion protein levels (Fig. 3). DLP1 levels were significantly increased in mitochondrial fraction of AD cybrids (~1.5–1.6 fold) as compared to non-AD mitochondrial fraction. Accordingly, cytosolic DLP1 was reduced in AD cybrids (Fig. 3*A*,*C*). Mfn2 that controls mitochondrial fusion was significantly decreased in mitochondrial and increased in cytosolic fraction of AD cybrids (Fig. 3*B*,*D*). Thus, both fission and fusion protein levels were altered in a direction favoring mitochondrial fission in AD-derived mitochondria.

3.3 Effect of Antioxidant Treatment on Mitochondrial Function, Morphology, and Fission/Fusion Proteins in AD Cybrid Cells

In view of increased mitochondrial ROS in AD cybrids and an important contributor of oxidative stress to mitochondrial dysfunction and abnormal changes in mitochondrial structure [2, 4, 5], we next determined if antioxidant treatment could rescue altered mitochondrial function, morphology and fission/fusion dynamics. Cells were incubated with the antioxidant probucol, which prevents lipid and protein oxidation [4, 5]. Probucol treatment greatly attenuated mitochondrial ROS production/accumulation as shown by reduced Mitosox intensity compared to vehicle-treated AD cybrid cells (Fig. 4*A*). Such treatment significantly improved mitochondrial function and energy metabolism by increased membrane potential (as measured by TMRM staining), complex I activity, and ATP levels in AD cybrid cells (Fig. 4*B*–*E*). The protective effect of probucol on AD mitochondria-induced dysfunction suggests the involvement of oxidative stress in mitochondrial dysfunction.

We then evaluated the effect of probucol on mitochondrial density, length, and morphology. Mitochondria density was significantly increased in probucol treated AD cybrid cells compared to vehicle treatment (Fig. 4*F*). Similarly, the average mitochondrial length was increased in AD cybrids (Fig. 4*G*). Abnormal mitochondrial morphology in AD (fragmentation) cybrids was largely reversed compared to vehicle-treated AD cybrids (Fig. 4*H*), indicating the protective effect of antioxidant treatment on abnormal mitochondrial morphology. As shown in Fig. 4*I*–*J*, probucol treatment significantly increased Mfn2 and suppressed an increase in DLP1 expression in AD cybrids compared to the vehicle-treated cells. These data demonstrate that antioxidant reverses impaired mitochondrial fission and fusion dynamics in AD mitochondria.

3.4 Activation of ERK1/2 Signal Transduction is Responsible for Mitochondrial Fission/Fusion Proteins Translocation and Defects in Mitochondrial Function

Oxidative stress induces activation of MAP kinase including extracellular receptor kinase (ERK) and p38 [4, 29], which is linked to abnormal mitochondrial structure and function [4, 5, 30]. To examine the relatively unexplored role of ERK activation in AD-derived mitochondria, we first analyzed ERK1/2 phosphorylation by immunoblotting. AD cybrid cells exhibited significantly increased ERK1/2 phosphorylation (3–4 fold increase *vs.* non-AD neurons). Addition of PD98059, a specific ERK inhibitor, largely abolished ERK1/2 phosphorylation (Fig. 5*A*). A total ERK1/2 was not significantly changed in AD cybrids compared to non-AD cybrids. To determine the effect of oxidative stress on ERK1/2

activation, cells were treated with probucol and then analyzed for phospho-ERK1/2. Compared to vehicle treatment, probucol treatment significantly inhibited ERK1/2 phosphorylation in AD cybrid cells (Fig. 5*B*). The addition of PD98059 to the AD cybrid cells blocked mitochondrial ROS generation (Fig. 5*C*). To assess if there is a direct link of ERK1/2 activation to mitochondrial function, we examined the effect of ERK1/2 inhibitor on mitochondrial membrane potential. Treatment with PD98059 resulted in a significantly higher intensity of TMRM staining in AD cybrid cells than in vehicle-treated cells (Fig. 5*D*). These results demonstrate that, in AD cybrids, ERK signaling transduction was perturbed upon exposure to the oxidative stress.

Given that MAP Kinase signal pathway may be involved in regulating mitochondrial function and mitochondrial fission/fusion protein expression [31], we hypothesized that activation of the ERK pathway contributes to abnormal mitochondrial structure and function observed in AD cybrids. To test this concept, we evaluated mitochondrial morphology and mitochondrial fission/fusion protein expression levels in cybrid cells treated with PD98059. As shown in Fig. 5*E*, mitochondrial density was increased in AD cybrid cells treated with PD98059 compared to vehicle-treated cells. Similarly, PD98059 treatment increased mitochondrial length in AD cybrids (Fig. 5*F*). Morphologically, there was a significant reduction in mitochondrial fragmentation in AD cybrids (Fig. 5*G*). These data demonstrate that inhibition of ERK activation effectively rescues alterations in mitochondrial morphology in AD cybrids.

To explore the effect of ERK signal transduction on expression levels of mitochondrial fission/fusion proteins in AD cybrids, we immunoblotted mitochondrial fractions for DLP1 and Mfn2 expression as described above. Consistent with the results shown in Fig. 3, DLP1 levels in AD mitochondrial fraction were significantly increased (~1.5–1.6 fold). In contrast, PD98059 treatment reversed DLP1 expression levels compared to vehicle-treated cells (Fig. 5*H*), suggesting that inhibition of ERK activation rescues abnormal mitochondrial dynamics.

3.5 Treatment with Mitochondrial Division Inhibitor mdivi-1, DLP1^{K38A} or siRNA-DLP1 Rescues Perturbations of Mitochondrial Function and Mitochondrial Fission/fusion Events in AD Cybrids

Perturbed balance of mitochondrial fission and fusion is likely an important mechanism for mitochondrial and neuronal dysfunction in AD brain [15, 17]. Results presented above raise the question of whether such imbalance in mitochondrial fission/fusion in AD cybrids affects mitochondrial function, and whether inhibition of mitochondrial division rescues mitochondrial function defects. To address these questions, we investigated the effect of mitochondrial division inhibitor, mdivi-1, a selective inhibitor of GTPase activity in DLP1 [32]. Treatment with mdivi-1 blocked mitochondrial fragmentation and improved mitochondrial function induced by AD-derived mitochondrial defects. Mitochondrial length and density were significantly increased in mdivi-1 treated AD cybrid neurons, as compared to vehicle-treated cells (Fig. 6*A*–*B*). Accordingly, abnormal mitochondrial morphology was significantly eradicated with the treatment with mdivi-1, as shown by reduction of mitochondrial fragmentation in AD cybrids (Fig. 6*C*). Next, we evaluated mitochondrial respiration chain activity and bioenergetic ability following treatment with mdivi-1. Deficits

in complex IV activity and ATP levels were reversed by mdivi-1 treatment (Fig. 6*D–E*). Consistent with these results, AD cybrid cells showed a significant increase in mitochondrial membrane potential when exposed to mdivi-1 (Fig. 6*F*). Addition of mdivi-1 also significantly suppressed ROS production in AD cybrids (Fig. 6*G–H*). Collectively, our data indicate that mdivi-1 confers protective effects on mitochondrial structure and function relevant to AD-derived mitochondrial toxicity.

To further validate the effect of DLP1 on abnormal mitochondrial dynamics that result in mitochondrial morphological changes, we introduced a dominant negative protein defective in GTP binding (DLPl^{K38A}) to inhibit DLP1 GTPase activity or siRNA-targeted DLP1 to knockdown DLP1 expression in AD cybrid cells. AD cybrid cells expressing DLP1^{K38A} rescued mitochondrial morphology as shown by the elongated mitochondria and reduced mitochondrial fragmentation compared to empty vector transfected AD cybrid neurons (Fig. 7*A–C*). DLP1^{K38A}-transfected cells increased CcO activity (Fig. 7*D*). Similar results were obtained from siRNA-DLP1 treated cells (Fig. 7*E–J*). AD cells with reduced levels of DLP1 had an increase in the average of mitochondrial length and density as well as mitochondrial membrane potential and ATP levels compared to the control siRNA treated cells. These results indicate that disruption of DLP1 expression in AD- derived mitochondria may be responsible for abnormal mitochondrial structure and function. We further tested whether the blockade of DLP1 by pharmaceutical inhibitors or genetic knockdown of DLP1 affected the ERK signaling in AD cybrids. There were no significant changes on phosphorylation and expression levels of ERK1/2 under mdivi-1/ DLP1K38A/ siRNA-DLP1 experimental conditions (Fig. S4), indicating that activation of ERK signaling may serve as an upstream regulator of the ERK-DLP-1 pathway.

4. Discussion

Although abnormalities in mitochondrial structure and function in AD brain and AD mouse models are well documented [2, 24, 33–35], the underlying mechanisms and the strategy to rescue mitochondrial degeneration remain elusive. Particularly, the status of mitochondrial fusion and fission pathway and its relationship between mitochondrial bioenergy and mitochondrial morphology in human AD mitochondria have not been fully elucidated. Here, we demonstrated the functional and metabolic differences in AD-derived mitochondria in cybrid cells and the potential mechanisms by which AD mitochondria regulates mitochondrial fission/fusion event through oxidative stress mediated activation of ERK-DLP1 signal transduction.

First, we validated the consequence and impact of AD-derived mitochondrial defects on mitochondrial structure and function using cybrid cell lines containing platelet mitochondria from AD and age-matched subjects to repopulate mtDNA-free Rho^0 neuroblastoma cells. The resulting AD and non-AD cybrid cells have the same nuclear DNA background at the time of experiments. Consistent with the previous report, these human neuronal cybrids recapitulate many features observed in AD brain including impaired mitochondrial respiratory function as shown by decreased enzyme activity associated with respiratory chain [36, 37], decreased membrane potential and ATP levels, and increased mitochondrial oxidative stress [38, 39]. The complex III activity was also declined in the platelet and

lymphocyte prepared from AD patients [8]. Although there was one report that there is no difference in the amount of complex III between AD and non-AD control brains [40], the complex III activity could be significantly altered. For example, complex III activity was significantly decreased in the brain of transgenic AD mouse model [24]. Thus, it requires further investigation to analyze whether complex III enzyme activity is altered in AD affected brain. Nevertheless, by using cybrid cells generated by fusing the Rho0 cells with the AD-derived platelet mitochondria, we observe deficits in enzymatic activity associated with respiratory chain including complex III, which is consistent with defect of complex III activity founded in the platelet from AD patients [8].

Second, we demonstrated significant changes in mitochondrial morphology and fission/fusion balance in AD cybrids. Defects in mitochondrial structure and function observed in AD cybrid cells associate with altered expression and distribution of Mfn2 or DLP1. Third, the structural and functional defects caused by AD mitochondria are protected by antioxidant and inhibition of ERK1/2 activation. Importantly, pharmacological blockade of mitochondrial division using mdivi-1, an inhibitor of DLP1 GTPase, and genetic restoration with dominant negative $DLP1^{K38A}$ and knockdown of DLP1 expression rescue mitochondrial morphology and function. Our current study provides new insights into the human AD mitochondria-mediated structural and functional changes and identifies a potential protective therapy against mitochondrial degeneration and improvement of mitochondrial function relevant to the AD pathogenesis.

Morphologically, AD cybrids had fragmented, misshaped, and bleb-like mitochondria, which are consistent with alterations in ultrastructure observed in AD neurons from human brain and mouse models [30, 34, 35]. AD cybrid cells had lower mitochondrial density compared to non-AD cybrids. To evaluate the possible effect on autophage/mitophagy, we have performed immunostaining and immunoblotting of cybrid cells with autophagy marker Light Chain (LC3). There are no significant changes in LC3 expression level or its activation (Fig. S3), suggesting that there is no significant autophagy occurring in non-AD or AD cybrid cells and that the mitochondrial density change may not associate with mitophagy.

We explored the involvement of abnormal mitochondrial dynamics by investigating changes in expression of mitochondrial fission and fusion proteins. AD cybrid cells showed an increased DLP1 translocation to mitochondria, whereas Mfn2 expression was decreased in AD cybrid mitochondria, suggesting that abnormal balance of mitochondrial fission and fusion in AD cybrids. DLP1 exists primarily in the cytoplasm but partially associates into foci on the outer surface of mitochondria that coalesce at sites of mitochondrial fission [28]. Increased DLP1 recruitment to mitochondria results in higher rates of DLP1-dependent mitochondrial division and mitochondrial fragmentation [15]. Therefore, changes in DLP1 expression levels and distribution as well as changes in other fusion proteins, such as Mfn2, likely contribute to enhanced mitochondrial fission, which may in turn be responsible for fragmentation of mitochondria observed in AD cybrids.

Given that oxidative stress disrupts mitochondrial structure and function [2, 4, 5], we assess whether antioxidant rescues oxidative stress-induced aberrant mitochondrial morphology

and function. Probucol is an antioxidant preventing protein or lipid peroxidation and has been clinically used during the past few decades for the treatment and prevention of cardiovascular disease [41, 42]. Further, the addition of probucol attenuates Aβ- or AGE-induced oxidative stress [4, 5, 43] and protects against ischemia-induced neuronal injury [4, 44]. Indeed, treatment with probucol significantly blunted mitochondrial ROS production, and augmented mitochondrial membrane potential, respiratory chain complexes activities and ATP production. Although the disruption of mitochondrial fission and fusion status in Huntington's disease is associated with increased ROS [45], to our knowledge this is the first demonstration of the contribution of mitochondrial ROS to dysregulation of mitochondrial fission and fusion induced by AD-derived mitochondria. Probucol treatment rescued abnormal mitochondrial morphology by controlling mitochondrial fission and fusion balance and associated protein expression levels, indicating that increased oxidative stress in AD mitochondria is responsible for the perturbation of mitochondrial dynamics leading to aberrant mitochondrial structure and function.

Activation of the MAP kinases ERK is associated with increased oxidative stress as well as mitochondrial and neuronal stress [29, 46, 47]. We found that ERK1/2 phosphorylation was significantly increased in AD cybrid cells. The antioxidant probucol blocked ERK1/2 activation along with attenuating mitochondrial perturbation, suggesting the impact of oxidative stress on ERK signal transduction, leading to mitochondrial injury.

ERK activation correlates with increased mitochondrial fission and DLP1 translocation in α-synuclein-mediated changes in mitochondrial dynamics [48]. Little is known about the ERK signal-transduction pathways that may regulate mitochondrial fission/fusion dynamics in AD-derived mitochondria. Given that blockade of ERK1/2 activation rescues mitochondrial morphology by suppressing mitochondrial DLP1 levels in AD cybrids, we propose that oxidative stress-mediated ERK activation augments DLP1 recruitment to mitochondria and shifts mitochondrial dynamics toward excessive fission in AD, contributing to abnormal mitochondrial morphology such as fragmentation of mitochondria. Abnormalities in mitochondrial fission/fusion equilibrium precede functional defects in AD animal models. Indeed, ERK inhibition accompanies functional recovery thereby supporting a pivotal upstream role for ERK in regulation of mitochondrial function through influence on mitochondrial dynamics. Taken together, we provide evidence that an axis of oxidative stress, ERK and DLP1 signal transduction are critical to AD-related mitochondrial dynamic imbalance and dysfunction (Fig. 8).

Inhibition of mitochondrial division using small molecule inhibitors (i.e., mdivi-1) in PD and HD cell culture models or dominant negative forms of DLP1 in Aβ-impaired cell culture models attenuates disease associated phenotypes [49–52]. Whether and how attenuation of higher rates of mitochondrial division rescues defects associated with AD-derived mitochondria has not yet been reported. In view of increased mitochondrial fraction of DLP1 in AD cybrid and a key player of DLP1 in maintaining normal mitochondrial dynamics, we examined the effect of mdivi-1, a selective inhibitor of GTPase activity in DLP1 [32], on aberrant mitochondrial morphology and function. Treatment with mdivi-1 protects neurons from AD mitochondria-mediated injury. Furthermore, introduction of $DLP1^{K38A}$, or siRNA-DLP1 attenuated abnormal mitochondrial morphology and improved

mitochondrial function, as shown by resultant inhibition of mitochondrial fragmentation, and improved mitochondrial respiratory function and bioenergy. These data suggest that blockade of DLP1 by pharmaceutical inhibitors or genetic knockdown of DLP1 can rescue perturbation of mitochondrial defects. Taken together, our data support that DLP1 plays a critical role in mitochondrial dynamic imbalance insulted by AD-derived mitochondria. The protective effect of DLP1 on mitochondrial toxicity in human AD-derived mitochondria suggests DLP1 as a potential and novel therapeutic target for AD.

In summary, our data offer new insights into structural and functional defects of human AD mitochondria and the associated ERK-DLP1 signaling pathway. We provide substantial evidence that the ERK pathway is involved in oxidative stress-induced DLP1 translocation to mitochondria in AD cybrids. We hypothesize that increased oxidative stress in AD mitochondria activates ERK signal transduction, disrupts mitochondrial fission and fusion balance, and promotes translocation of DLP1 to mitochondria, leading to mitochondrial fragmentation in AD. Most importantly, suppression of ERK signaling and inhibition of mitochondrial fission pathways restore mitochondrial morphology and function induced by AD mitochondrial defects (Fig.8). Thus, small molecule targeting to mitochondrial fission (i.e., mdivi-1) may be a significant novel therapeutic strategy for AD treatment.

Supplementary Material

Refer to Web version on PubMed Central for supplementary material.

Acknowledgments

This study was supported by grants from the National Institute of Aging (R37AG037319), National Institute of General Medical Science (R01GM095355), and the University of Kansas Alzheimer’s Disease Center (NIA P30AG035982).

Reference

1. Swerdlow RH. Mitochondria and cell bioenergetics: increasingly recognized components and a possible etiologic cause of Alzheimer's disease. Antioxidants & redox signaling. 2012; 16:1434–1455. [PubMed: 21902597]
2. Du H, Guo L, Fang F, Chen D, Sosunov AA, McKhann GM, Yan Y, Wang C, Zhang H, Molkentin JD, Gunn-Moore FJ, Vonsattel JP, Arancio O, Chen JX, Yan SD. Cyclophilin D deficiency attenuates mitochondrial and neuronal perturbation and ameliorates learning and memory in Alzheimer's disease. Nat Med. 2008; 14:1097–1105. [PubMed: 18806802]
3. Du H, Guo L, Yan SS. Synaptic Mitochondrial Pathology in Alzheimer's Disease. Antioxid Redox Signal. 2011
4. Guo L, Du H, Yan S, Wu X, McKhann GM, Chen JX, Yan SS. Cyclophilin D deficiency rescues axonal mitochondrial transport in Alzheimer's neurons. PLoS One. 2013; 8:e54914. [PubMed: 23382999]
5. Du H, Guo L, Wu X, Sosunov AA, McKhann GM, Chen JX, Yan SS. Cyclophilin D deficiency rescues Abeta-impaired PKA/CREB signaling and alleviates synaptic degeneration. Biochim Biophys Acta. 2013
6. Lin MT, Beal MF. Alzheimer's APP mangles mitochondria. Nat Med. 2006; 12:1241–1243. [PubMed: 17088888]
7. Swerdlow RH. Mitochondria and cell bioenergetics: increasingly recognized components and a possible etiologic cause of Alzheimer's disease. Antioxidants & redox signaling. 2012; 16:1434–1455. [PubMed: 21902597]

8. Valla J, Schneider L, Niedzielko T, Coon KD, Caselli R, Sabbagh MN, Ahern GL, Baxter L, Alexander G, Walker DG, Reiman EM. Impaired platelet mitochondrial activity in Alzheimer's disease and mild cognitive impairment. Mitochondrion. 2006; 6:323–330. [PubMed: 17123871]

9. Swerdlow RH, Kish SJ. Mitochondria in Alzheimer's disease. International review of neurobiology. 2002; 53:341–385. [PubMed: 12512346]

10. Chen JX, Yan SS. Role of mitochondrial amyloid-beta in Alzheimer's disease. J Alzheimers Dis. 2010; 20(Suppl 2):S569–S578. [PubMed: 20463403]

11. Pellerin L, Magistretti PJ. Food for thought: challenging the dogmas. Journal of cerebral blood flow and metabolism : official journal of the International Society of Cerebral Blood Flow and Metabolism. 2003; 23:1282–1286.

12. Chan DC. Mitochondria: dynamic organelles in disease, aging, and development. Cell. 2006; 125:1241–1252. [PubMed: 16814712]

13. McBride HM, Neuspiel M, Wasiak S. Mitochondria: more than just a powerhouse. Curr Biol. 2006; 16:R551–R560. [PubMed: 16860735]

14. Frazier AE, Kiu C, Stojanovski D, Hoogenraad NJ, Ryan MT. Mitochondrial morphology and distribution in mammalian cells. Biol Chem. 2006; 387:1551–1558. [PubMed: 17132100]

15. Wang X, Su B, Lee HG, Li X, Perry G, Smith MA, Zhu X. Impaired balance of mitochondrial fission and fusion in Alzheimer's disease. The Journal of neuroscience : the official journal of the Society for Neuroscience. 2009; 29:9090–9103. [PubMed: 19605646]

16. Wang X, Su B, Siedlak SL, Moreira PI, Fujioka H, Wang Y, Casadesus G, Zhu X. Amyloid-beta overproduction causes abnormal mitochondrial dynamics via differential modulation of mitochondrial fission/fusion proteins. Proceedings of the National Academy of Sciences of the United States of America. 2008; 105:19318–19323. [PubMed: 19050078]

17. Wang X, Su B, Zheng L, Perry G, Smith MA, Zhu X. The role of abnormal mitochondrial dynamics in the pathogenesis of Alzheimer's disease. Journal of neurochemistry. 2009; 109(Suppl 1):153–159. [PubMed: 19393022]

18. Silva DF, Santana I, Esteves AR, Baldeiras I, Arduino DM, Oliveira CR, Cardoso SM. Prodromal Metabolic Phenotype in MCI Cybrids: Implications for Alzheimers Disease. Current Alzheimer research. 2012

19. Khan SM, Cassarino DS, Abramova NN, Keeney PM, Borland MK, Trimmer PA, Krebs CT, Bennett JC, Parks JK, Swerdlow RH, Parker WD Jr, Bennett JP Jr. Alzheimer's disease cybrids replicate beta-amyloid abnormalities through cell death pathways. Annals of neurology. 2000; 48:148–155. [PubMed: 10939564]

20. Fratiglioni L, Grut M, Forsell Y, Viitanen M, Winblad B. Clinical diagnosis of Alzheimer's disease and other dementias in a population survey. Agreement and causes of disagreement in applying Diagnostic and Statistical Manual of Mental Disorders. Criteria, Archives of neurology (Revised Third Edition). 1992; 49:927–932.

21. Miller SW, Trimmer PA, Parker WD Jr, Davis RE. Creation and characterization of mitochondrial DNA-depleted cell lines with "neuronal-like" properties. Journal of neurochemistry. 1996; 67:1897–1907. [PubMed: 8863494]

22. Swerdlow RH. Mitochondria in cybrids containing mtDNA from persons with mitochondriopathies. Journal of neuroscience research. 2007; 85:3416–3428. [PubMed: 17243174]

23. Tieu K, Perier C, Caspersen C, Teismann P, Wu DC, Yan SD, Naini A, Vila M, Jackson-Lewis V, Ramasamy R, Przedborski S. D-beta-hydroxybutyrate rescues mitochondrial respiration and mitigates features of Parkinson disease. J Clin Invest. 2003; 112:892–901. [PubMed: 12975474]

24. Caspersen C, Wang N, Yao J, Sosunov A, Chen X, Lustbader JW, Xu HW, Stern D, McKhann G, Yan SD. Mitochondrial Abeta: a potential focal point for neuronal metabolic dysfunction in Alzheimer's disease. FASEB J. 2005; 19:2040–2041. [PubMed: 16210396]

25. Du H, Guo L, Yan S, Sosunov AA, McKhann GM, Yan SS. Early deficits in synaptic mitochondria in an Alzheimer's disease mouse model. Proc Natl Acad Sci U S A. 2010; 107:18670–18675. [PubMed: 20937894]

26. Chou CH, Lin CC, Yang MC, Wei CC, Liao HD, Lin RC, Tu WY, Kao TC, Hsu CM, Cheng JT, Chou AK, Lee CI, Loh JK, Howng SL, Hong YR. GSK3beta-mediated Drp1 phosphorylation

induced elongated mitochondrial morphology against oxidative stress. PloS one. 2012; 7:e49112. [PubMed: 23185298]

27. Mozdy AD, Shaw JM. A fuzzy mitochondrial fusion apparatus comes into focus, Nature reviews. Molecular cell biology. 2003; 4:468–478. [PubMed: 12778126]
28. Smirnova E, Griparic L, Shurland DL, van der Bliek AM. Dynamin-related protein Drp1 is required for mitochondrial division in mammalian cells. Molecular biology of the cell. 2001; 12:2245–2256. [PubMed: 11514614]
29. Arancio O, Zhang HP, Chen X, Lin C, Trinchese F, Puzzo D, Liu S, Hegde A, Yan SF, Stern A, Luddy JS, Lue LF, Walker DG, Roher A, Buttini M, Mucke L, Li W, Schmidt AM, Kindy M, Hyslop PA, Stern DM, Du Yan SS. RAGE potentiates Abeta-induced perturbation of neuronal function in transgenic mice. Embo J. 2004; 23:4096–4105. [PubMed: 15457210]
30. Yu T, Jhun BS, Yoon Y. High-glucose stimulation increases reactive oxygen species production through the calcium and mitogen-activated protein kinase-mediated activation of mitochondrial fission. Antioxidants & redox signaling. 2011; 14:425–437. [PubMed: 20518702]
31. Rasola A, Sciacovelli M, Chiara F, Pantic B, Brusilow WS, Bernardi P. Activation of mitochondrial ERK protects cancer cells from death through inhibition of the permeability transition. Proc Natl Acad Sci U S A. 2010; 107:726–731. [PubMed: 20080742]
32. Cassidy-Stone A, Chipuk JE, Ingerman E, Song C, Yoo C, Kuwana T, Kurth MJ, Shaw JT, Hinshaw JE, Green DR, Nunnari J. Chemical inhibition of the mitochondrial division dynamin reveals its role in Bax/Bak-dependent mitochondrial outer membrane permeabilization. Dev Cell. 2008; 14:193–204. [PubMed: 18267088]
33. Chen JX, Yan SD. Amyloid-beta-induced mitochondrial dysfunction. J Alzheimers Dis. 2007; 12:177–184. [PubMed: 17917162]
34. Du H, Yan SS. Mitochondrial medicine for neurodegenerative diseases. Int J Biochem Cell Biol. 2010; 42:560–572. [PubMed: 20067840]
35. Lustbader JW, Cirilli M, Lin C, Xu HW, Takuma K, Wang N, Caspersen C, Chen X, Pollak S, Chaney M, Trinchese F, Liu S, Gunn-Moore F, Lue LF, Walker DG, Kuppusamy P, Zewier ZL, Arancio O, Stern D, Yan SS, Wu H. ABAD directly links Abeta to mitochondrial toxicity in Alzheimer's disease. Science. 2004; 304:448–452. [PubMed: 15087549]
36. Kim SH, Vlkolinsky R, Cairns N, Fountoulakis M, Lubec G. The reduction of NADH ubiquinone oxidoreductase 24- and 75-kDa subunits in brains of patients with Down syndrome and Alzheimer's disease. Life sciences. 2001; 68:2741–2750. [PubMed: 11400916]
37. Fukuyama R, Hatanpaa K, Rapoport SI, Chandrasekaran K. Gene expression of ND4, a subunit of complex I of oxidative phosphorylation in mitochondria, is decreased in temporal cortex of brains of Alzheimer's disease patients. Brain research. 1996; 713:290–293. [PubMed: 8725003]
38. Zhang H, Liu Y, Lao M, Ma Z, Yi X. Puerarin protects Alzheimer's disease neuronal cybrids from oxidant-stress induced apoptosis by inhibiting pro-death signaling pathways. Experimental gerontology. 2011; 46:30–37. [PubMed: 20933077]
39. Cardoso SM, Santana I, Swerdlow RH, Oliveira CR. Mitochondria dysfunction of Alzheimer's disease cybrids enhances Abeta toxicity. J Neurochem. 2004; 89:1417–1426. [PubMed: 15189344]
40. Schagger H, Ohm TG. Human diseases with defects in oxidative phosphorylation. 2. F1F0 ATP-synthase defects in Alzheimer disease revealed by blue native polyacrylamide gel electrophoresis. European journal of biochemistry / FEBS. 1995; 227:916–921. [PubMed: 7867655]
41. Buckley MM, Goa KL, Price AH, Brogden RN. Probucol. A reappraisal of its pharmacological properties and therapeutic use in hypercholesterolaemia. Drugs. 1989; 37:761–800. [PubMed: 2667936]
42. Yamashita S, Matsuzawa Y. Where are we with probucol: a new life for an old drug? Atherosclerosis. 2009; 207:16–23. [PubMed: 19457483]
43. Yan SD, Schmidt AM, Anderson GM, Zhang J, Brett J, Zou YS, Pinsky D, Stern D. Enhanced cellular oxidant stress by the interaction of advanced glycation end products with their receptors/binding proteins. J Biol Chem. 1994; 269:9889–9897. [PubMed: 8144582]
44. Farina M, Campos F, Vendrell I, Berenguer J, Barzi M, Pons S, Sunol C. Probucol increases glutathione peroxidase-1 activity and displays long-lasting protection against methylmercury

toxicity in cerebellar granule cells. Toxicological sciences : an official journal of the Society of Toxicology. 2009; 112:416–426. [PubMed: 19770487]

45. Liot G, Bossy B, Lubitz S, Kushnareva Y, Sejbuk N, Bossy-Wetzel E. Complex II inhibition by 3-NP causes mitochondrial fragmentation and neuronal cell death via an NMDA- and ROS-dependent pathway. Cell death and differentiation. 2009; 16:899–909. [PubMed: 19300456]
46. Dong XB, Yang CT, Zheng DD, Mo LQ, Wang XY, Lan AP, Hu F, Chen PX, Feng JQ, Zhang MF, Liao XX. Inhibition of ROS-activated ERK1/2 pathway contributes to the protection of H2S against chemical hypoxia-induced injury in H9c2 cells. Molecular and cellular biochemistry. 2012; 362:149–157. [PubMed: 22134701]
47. Rasola A, Sciacovelli M, Chiara F, Pantic B, Brusilow WS, Bernardi P. Activation of mitochondrial ERK protects cancer cells from death through inhibition of the permeability transition. Proceedings of the National Academy of Sciences of the United States of America. 2010; 107:726–731. [PubMed: 20080742]
48. Gui YX, Wang XY, Kang WY, Zhang YJ, Zhang Y, Zhou Y, Quinn TJ, Liu J, Chen SD. Extracellular signal-regulated kinase is involved in alpha-synuclein-induced mitochondrial dynamic disorders by regulating dynamin-like protein 1. Neurobiology of aging. 2012; 33:2841–2854. [PubMed: 22445325]
49. Cui M, Tang X, Christian WV, Yoon Y, Tieu K. Perturbations in mitochondrial dynamics induced by human mutant PINK1 can be rescued by the mitochondrial division inhibitor mdivi-1. The Journal of biological chemistry. 2010; 285:11740–11752. [PubMed: 20164189]
50. Lutz AK, Exner N, Fett ME, Schlehe JS, Kloos K, Lammermann K, Brunner B, Kurz-Drexler A, Vogel F, Reichert AS, Bouman L, Vogt-Weisenhorn D, Wurst W, Tatzelt J, Haass C, Winklhofer KF. Loss of parkin or PINK1 function increases Drp1-dependent mitochondrial fragmentation. J Biol Chem. 2009; 284:22938–22951. [PubMed: 19546216]
51. Wang H, Lim PJ, Karbowski M, Monteiro MJ. Effects of overexpression of huntingtin proteins on mitochondrial integrity. Hum Mol Genet. 2009; 18:737–752. [PubMed: 19039036]
52. Cho DH, Nakamura T, Fang J, Cieplak P, Godzik A, Gu Z, Lipton SA. S-nitrosylation of Drp1 mediates beta-amyloid-related mitochondrial fission and neuronal injury. Science. 2009; 324:102–105. [PubMed: 19342591]

Abbreviations

AD	Alzheimer’s disease
mtDNA	Mitochondrial DNA
DLP1	dynamin-like protein
Mfn2	mitofusin 2
ERK	extracellular signal-regulated kinase
Aβ	amyloid beta peptide
CcO	Cytochrome c oxidase
ROS	reactive oxygen species
PD	Parkinson disease
HD	Huntington disease
TMRM	tetramethylrhodaminemethylester

Highlights

1. Imbalance of mitochondrial dynamics contributes to AD mitochondrial dysfunction
2. Activation of ERK/Dlp1 signaling disrupts proper mitochondrial dynamics
3. Antioxidant and suppressing ERK activation rescue mitochondrial morphology and function
4. Inhibition of excessive mitochondrial fission protects against AD mitochondrial defects

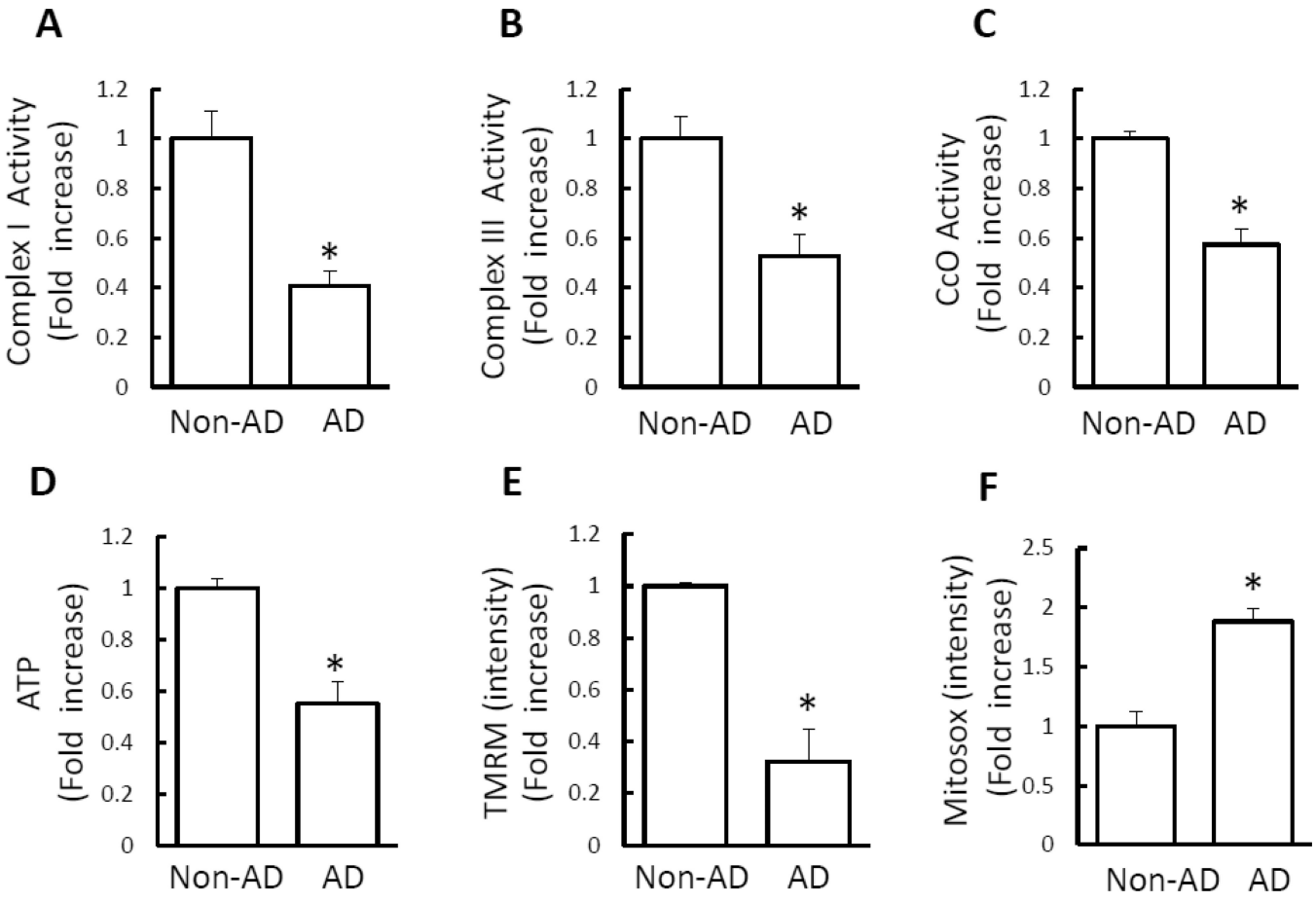

Figure 1.

Mitochondrial dysfunction in AD cybrid cells. **A–D)** Enzymatic activity of complex I, III, and IV (CcO), and ATP levels were determined in cell lysates from indicated cell groups. **E–F)** Mitochondrial membrane potential and reactive oxygen species (ROS) were measured by TMRM (**E**) and Mitosox staining intensity (**F**), respectively. Image intensity was quantified using NIH Image J software. Data are expressed as fold increase relative to non-AD cybrid cells. N = 7 cell lines/group. * $p<0.05$ *versus* non-AD group.

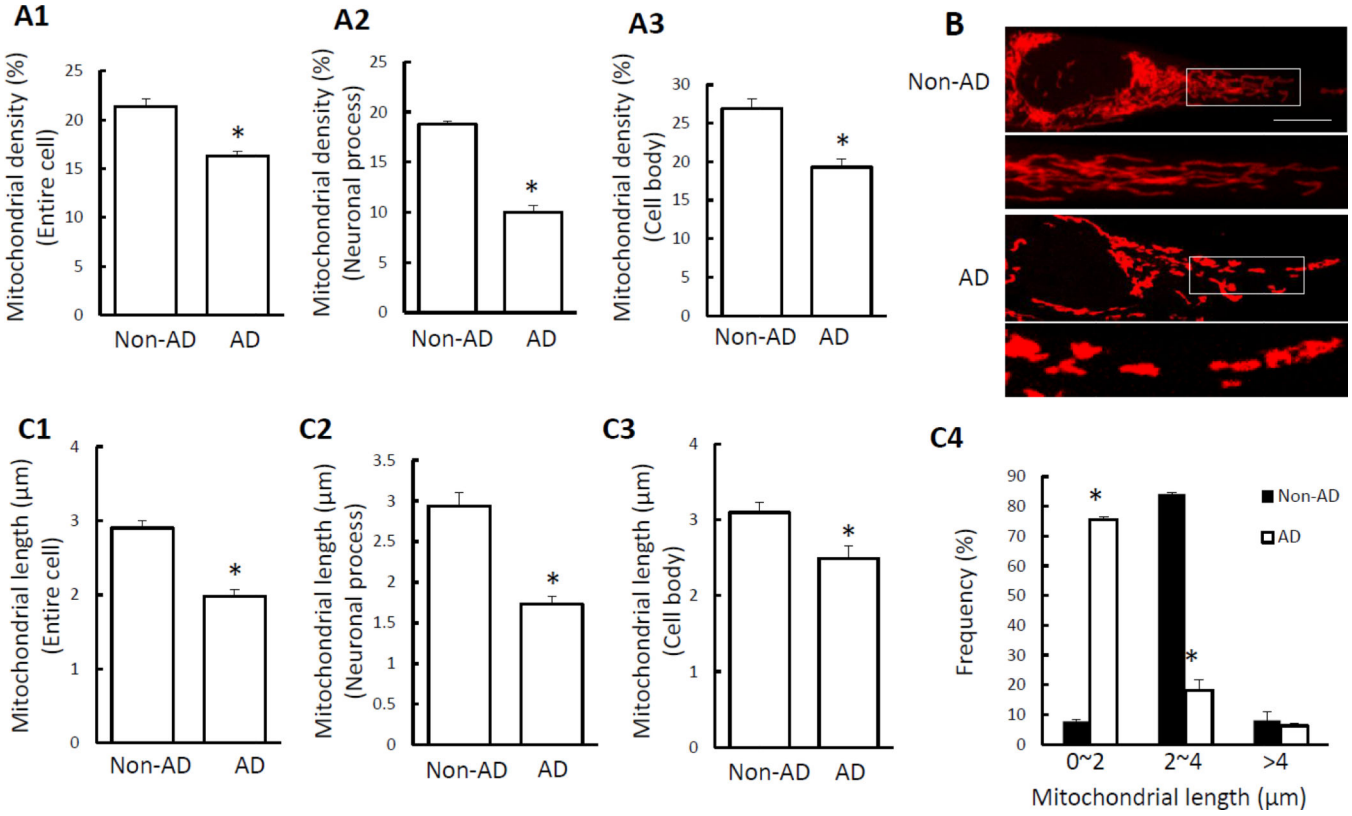

Figure 2.

Abnormal mitochondrial morphology in AD cybrid cells. Cybrid cells were labeled with Mitotracker Red for visualization of mitochondrial morphology. **(A1–A3)** Quantitative measurement of mitochondrial density presented as the percentage of area occupied by mitochondria in entire cells (**A1**), neuronal process (**A2**), or cell body (**A3**), using NIH Image J software. **B**) Representative images of Mitotracker Red staining. Lower panels present larger images corresponding to the indicated images above. Scale bar = 5 μm. (**C1–C3**) Average mitochondrial length over the entire cell, neuronal processes, and cell body was lower in AD cybrid cells compared to non-AD cells. (**C4**) Quantification of mitochondrial sizes based on the grouped differently sized bins. N = 7 cell lines/group. * $p<0.05$ *versus* non-AD group.

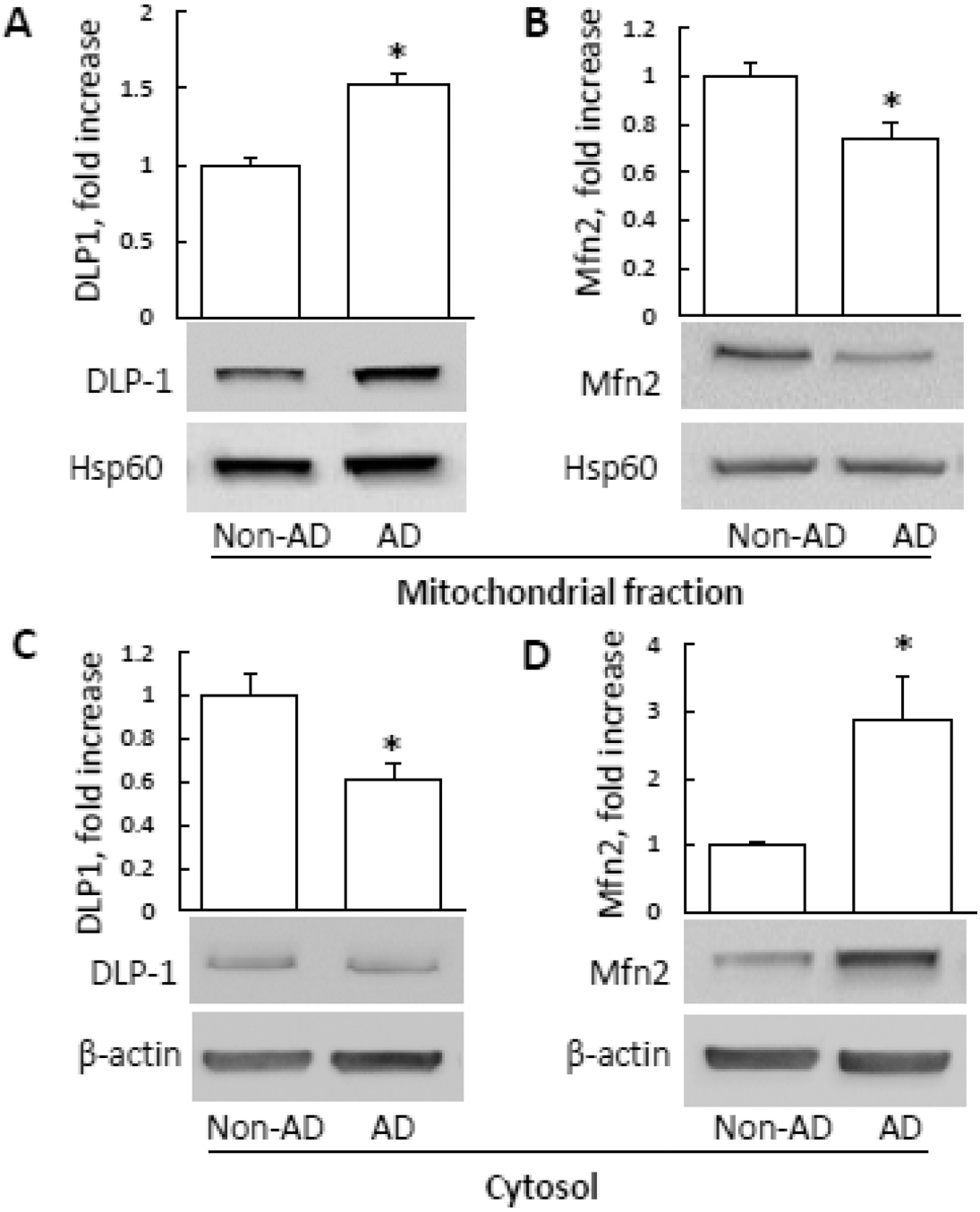

Figure 3.

DLP1 and Mfn2 expression levels in AD cybrid mitochondria. **A–D)** Densitometry of immunoreactive bands for DLP1 (**A, C**) and Mfn2 (**B, D**) in mitochondrial fractions (**A–B**) and cytosol (**C–D**) of indicated groups. Data were expressed as fold-increase of DLP1 or Mfn2 relative to non-AD cells. DLP1 or Mfn2 levels were normalized to mitochondrial marker Hsp60 or β-actin. Representative immunoblots are shown in lower panel. N = 7 cell lines/group. *$p<0.05$ *versus* non-AD group.

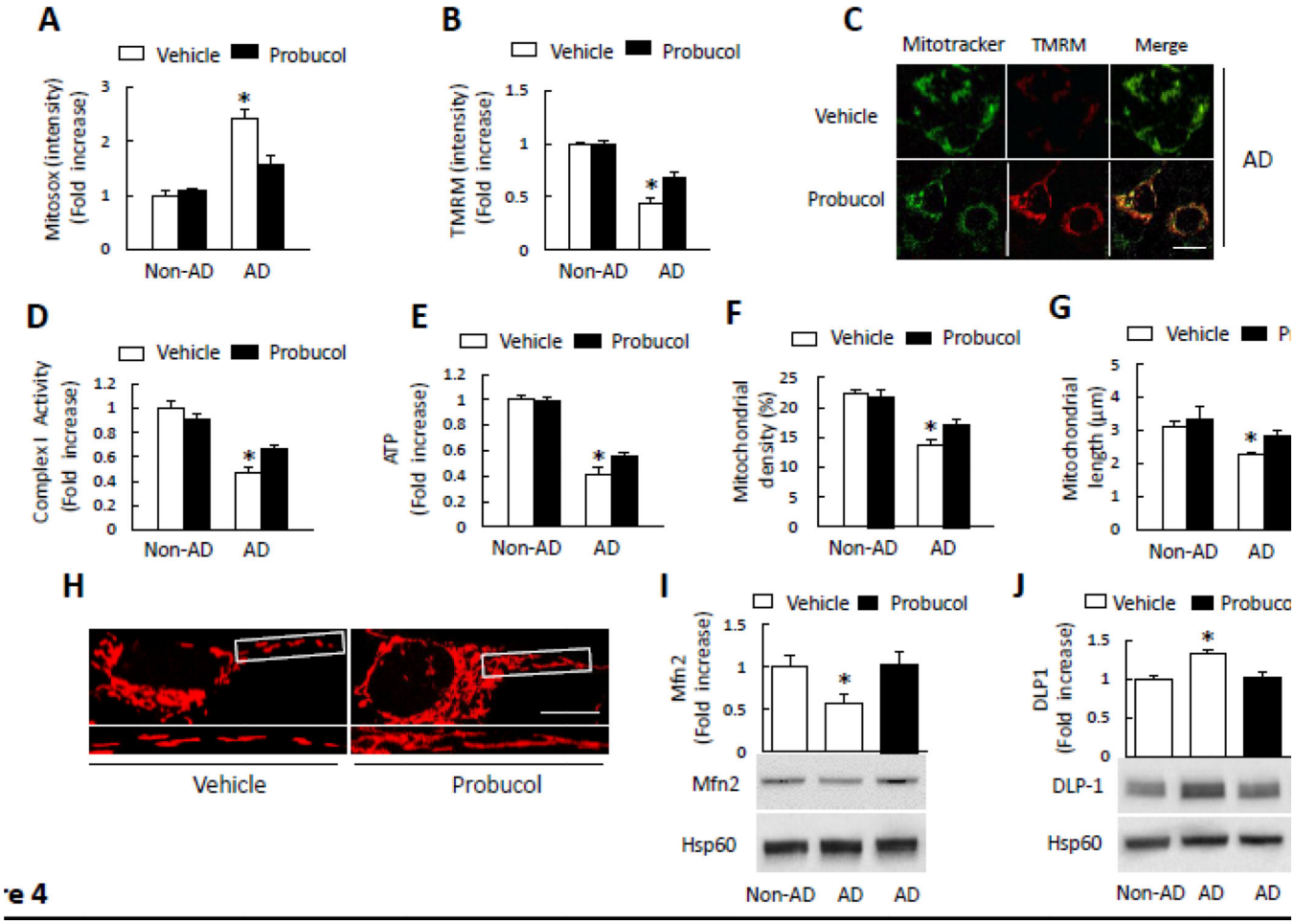

Figure 4.

Effect of antioxidant treatment on mitochondrial function and morphology. **A–B)** Cells were treated with probucol (10 μM) for 24 h and then stained with Mitosox or TMRM to determine mitochondrial ROS levels and membrane potential. Quantification of staining intensity for Mitosox (**A**) and TMRM (**B**) in the indicated groups of cells using NIH Image J software. *p<0.05 *versus* all non-AD groups and probucol treated AD group. (**C**) Representative images with TMRM staining (Scale bar = 10 μm). Mitotracker staining was used to show mitochondria. **D–E)** Complex I activity (**D**) and ATP levels (**E**) were measured in the indicated groups of cells with or without probucol treatment. Data are expressed as fold increase relative to vehicle-treated non-AD cybrid cells. *p<0.05 *versus* all non-AD groups and probucol treated AD group. **F–H)** Quantitative measurement of mitochondrial density (**F**) and average mitochondrial length (**G**) in indicated cell groups using NIH Image J. *p<0.05 *versus* all non-AD groups and probucol treated AD group. (**H**) Representative images of Mitotracker Red staining. The lower panels present larger images corresponding to indicated images above (Scale bar = 5μM). **I–J)** Quantification of immunoreactive bands for Mfn2 (**I**) or DLP1 (**J**) relative to Hsp60 in indicated cell groups with probucol or vehicle treatment using NIH Image J software. *, p<0.05 *versus* non-AD groups and probucol treated AD group. Data are expressed as fold increase relative to vehicle-treated non-AD

cybrid cells. Representative immunoblots are shown in the lower panel. N = 5–7 cell lines/group.

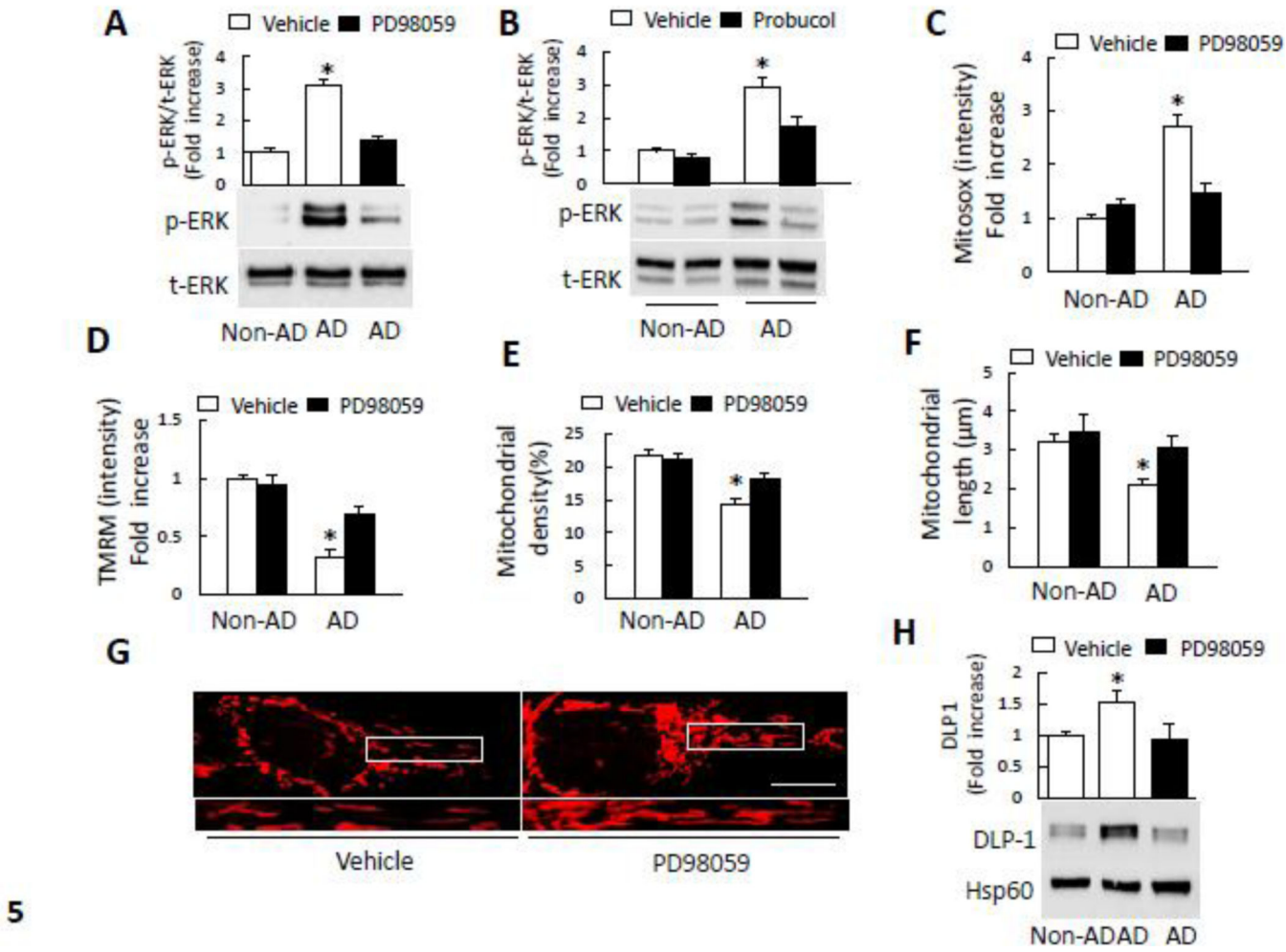

Figure 5.

Inhibition of ERK activation rescued abnormal mitochondrial function and morphology. **A–B)** Densitometry of immunoreactive bands for phospho-ERK1/2 (p-ERK1/2) using NIH Image J, normalized to total-ERK1/2 (t-ERK1/2) in indicated cell groups treated with PD98059 (10 μM for 2 h) (**A**), probucol (10 μM for 24 h) (**B**), or vehicle. **p*<0.05 *versus* all other groups. Representative immunoblots are shown in lower panel. **C)** PD98059 treatment decreased Mitosox staining intensity in AD cybrid cells compared to vehicle treatment. (**D**) TMRM staining intensity was significantly increased in AD cybrid cells treated with PD98059. **p*<0.05 *versus* all other groups. **E–F)** Effect of ERK inhibitor on mitochondrial morphology. Mitochondrial density (**E**) and average length (**F**) were measured in indicated cell groups treated with PD98059 or vehicle. **p*<0.05 *versus* all other groups. (**G)** Representative images are shown for Mitotracker Red staining. The lower panel is a larger image corresponding to the indicated image above (Scale bar = 5 μm). **H)** Quantification of immunoreactive bands for DLP1 and Mfn2 normalized to Hsp60 in mitochondrial fractions of the indicated cell groups with PD98059 or vehicle treatment. Representative immunoblots are shown in lower panel. Data are expressed as fold increase relative to vehicle-treated non-AD cybrid cells. **p*<0.05 *versus* all other groups. N = 5–7 cell lines/group.

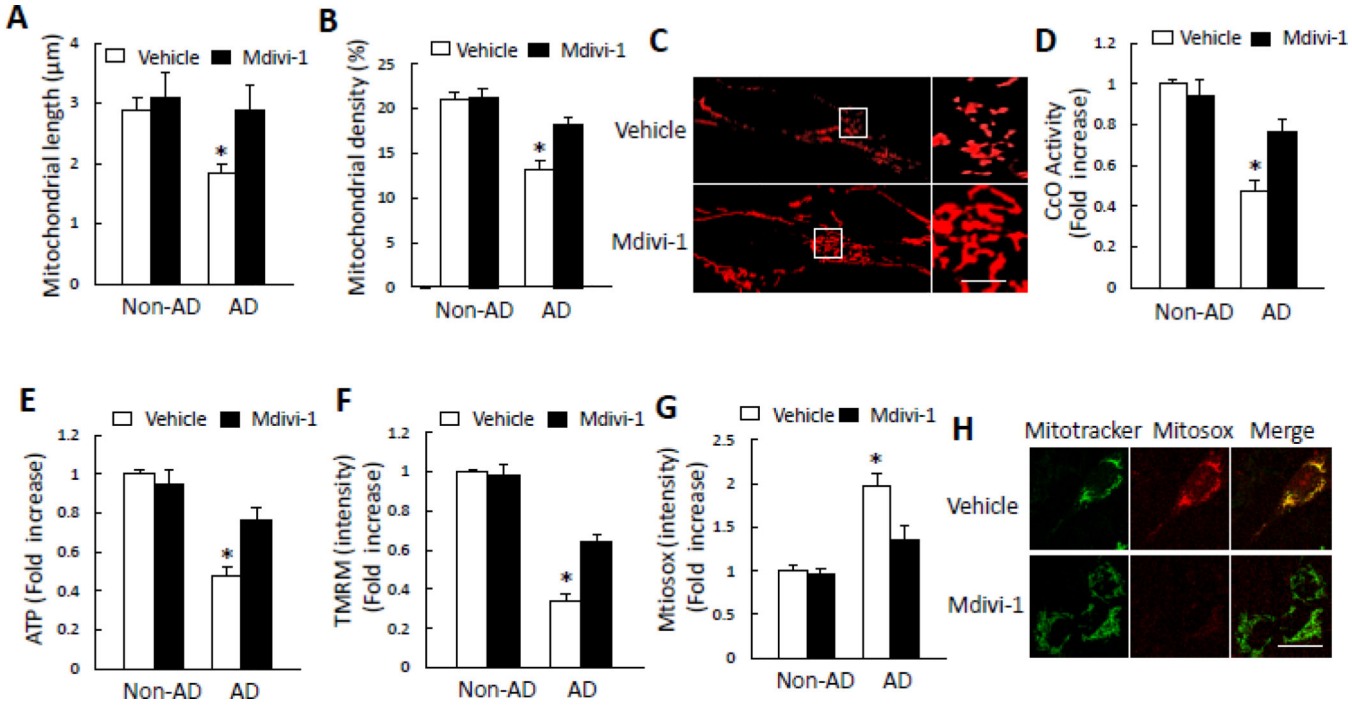

Figure 6.

Inhibition of DLP1 by mdivi-1 rescues mitochondrial structure and function in AD cybrid mitochondria. **A–C)** Effect of mdivi-1 on mitochondrial morphology. Mdivi-1 treatment (10 μM for 24 h) significantly increased mitochondrial length (**A**) and density (**B**) Representative images for Mitotracker red staining reveal mitochondrial morphology (**C**). **p*<0.05 *versus* all other groups. The right panel is a larger image corresponding to the indicated image on the left panel (Scale bar = 5 μm). **D–H)** Effect of mdivi-1 on mitochondrial function. Treatment with mdiv-1 resulted in increased CcO activity (**D**), ATP levels (**E**), and TMRM intensity in AD cybrid cells (**F**). Mdivi-1 also attenuated mitochondrial ROS production as shown by reduced level of Mitosox staining intensity (**G**) Representative images for Mitotracker and Mitosox staining are shown (**H**) (Scale bar = 10 μm). **p*<0.05 *versus* all other groups. N = 5–7 cell lines/group.

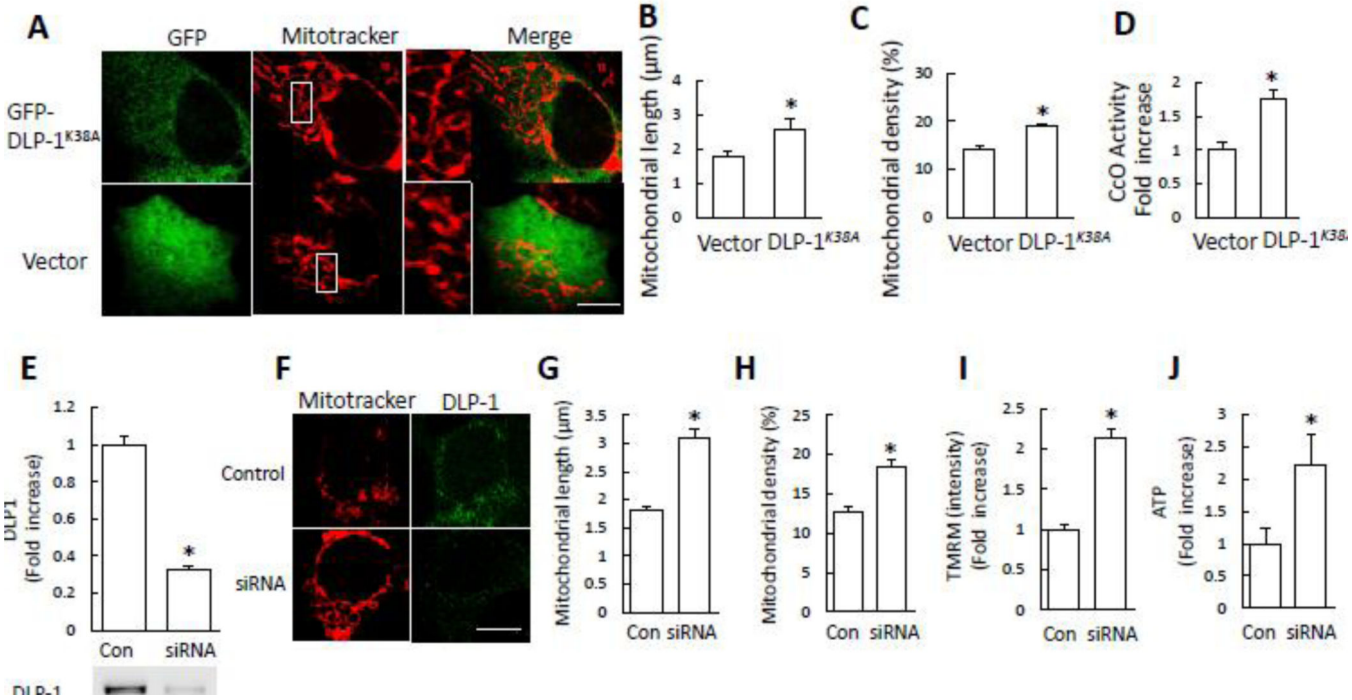

Figure 7.

Effect of DLP1 blockade accomplished by introduction of DLP1^{K38A} or siRNA-DLP1 to AD cybrid cells. **A–D)** AD cybrid cells were transfected with GFP-DLP1^{K38A} or empty vector. After 24 h, cells were incubated with Mitotracker Red to analyze mitochondrial morphology under confocal microscopy (Scale bar = 5 μm). DLP1^{K38A}-transfected AD cybrids had tubular mitochondria, whereas empty vector-transfected cells retained fragmented mitochondrial morphology (**A**). Mitochondrial average length (**B**), density (**C**), and CcO activity (**D**) were increased in DLP1^{K38A}-transfected cells compared to vector-transfected control cells. *p<0.05 *versus* vector treated group. **E–J)** Effect of siRNA-DLP1. Immunoblotting for DLP1 in cells treated with siRNA-DLP1 (siRNA) or control siRNA (con) (**E**). Representative immunoblots for DLP1 and β-actin. (**F**) Mitotracker staining and immunostaining of DLP1 in siRNA-DLP1 or control siRNA treated cells (Scale bar = 5 μm). Average mitochondrial length (**G**) and density (**H**).**I–J**), increased TMRM intensity (**I**), and ATP levels (**J**) in siRNA-DLP1 cells relative to control siRNA cells. *p<0.05 *versus* vector treated group. N = 5–7 cell lines/group.

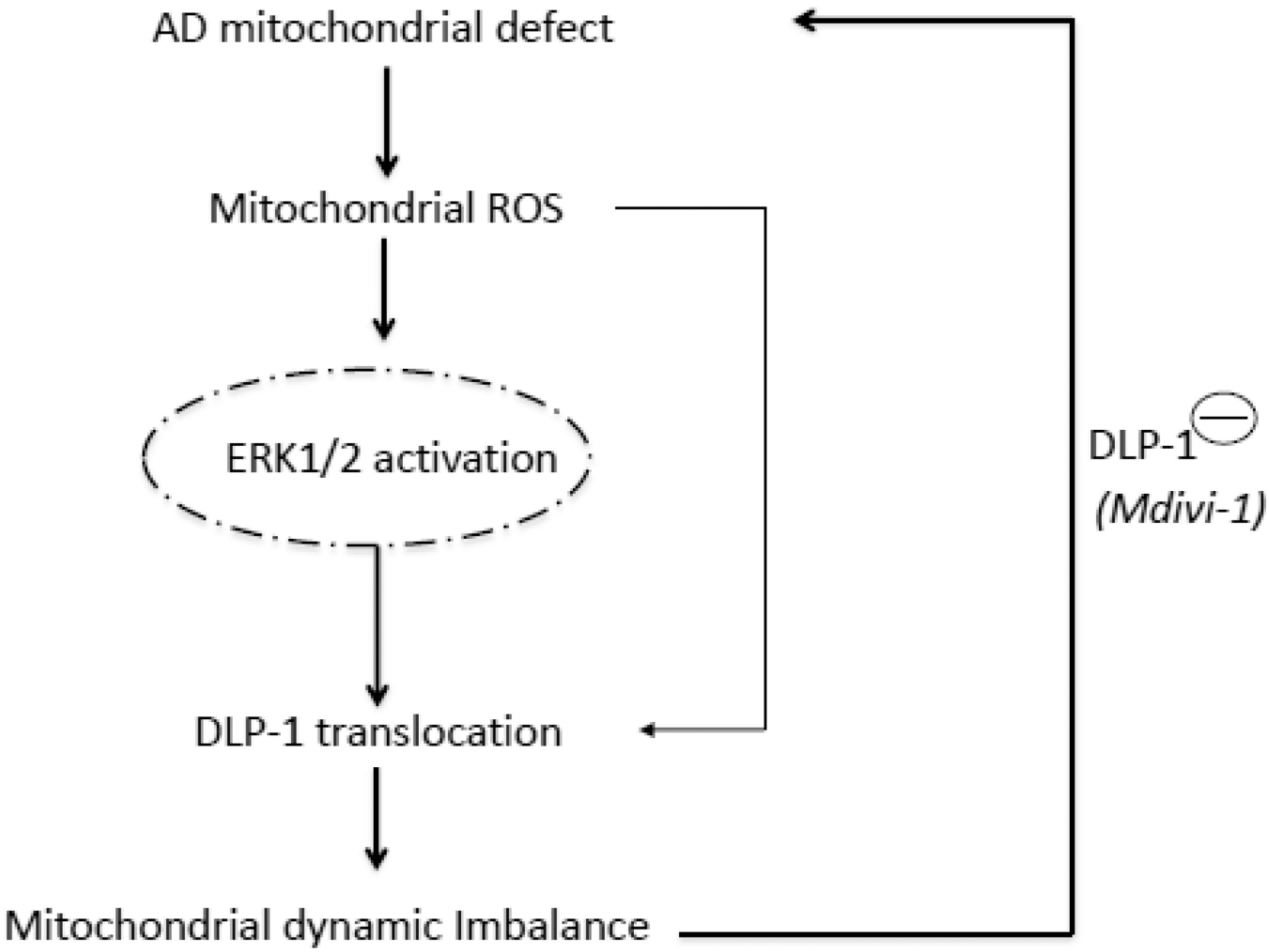

Figure 8.

Working hypothesis: Increased mitochondrial ROS generation/accumulation is due to defects in AD mitochondrial respiratory function, which leads to an activation of ERK signal transduction. ERK activation directly or indirectly disrupts the balance of mitochondrial dynamics (fusion and fission events) and results in altered DLP1 or Mfn2 expression levels and distribution, which eventually leads to aberrant mitochondrial morphology and function. Inhibition of DLP1 activity/expression levels by mdivi-1 or genetic blockade of DLP1 rescues the perturbation of mitochondrial morphology and function relevant to AD mitochondrial degeneration.